

Elsevier Editorial System(tm) for Journal of Non-Newtonian Fluid Mechanics
Manuscript Draft

Manuscript Number:

Title: Stress Communication and Filtering of Viscoelastic Layers in Oscillatory Shear

Article Type: Full Text Article

Keywords: Stress propagation; Large amplitude oscillatory shear; Shear waves; Upper convected Maxwell model; Biological layers.

Corresponding Author: Mr. Brandon Scott Lindley,

Corresponding Author's Institution: University of North Carolina

First Author: Brandon Scott Lindley

Order of Authors: Brandon Scott Lindley; Eddie L Howell III; Breannan D Smith; Gregory J Rubinstein; M. Gregory Forest; Sorin M Mitran; David B Hill; Richard Superfine

Abstract: We revisit a classical topic: response functions of viscoelastic layers in large amplitude oscillatory shear. Motivated by questions concerning biological layers, we focus on extreme values in boundary stress signals in a parallel plate geometry, and their dependence on material properties, layer thickness, or frequency of imposed strain. We identify a robust oscillatory structure in boundary stress signals, presented first in terms of a layer height sweep and then generalized to scaling behavior with respect to all experimental parameters. The structure consists of peaks and valleys in extreme values of shear and normal stress signals versus any parameter sweep, indicating redundant mechanisms for stress communication (by tuning to the peaks) and stress filtering (by tuning to the valleys). In this paper, we first restrict to a single mode nonlinear Maxwell model, where analysis renders a transparent explanation and simplified computation of the phenomena. We close with a Giesekus model simulation of coupled nonlinear partial differential equations, which is the context in which the phenomena was discovered. The analysis and simulations rely on and extend our recent studies of shear waves in a micro-parallel-plate rheometer.



UNC
COLLEGE OF
ARTS & SCIENCES

THE UNIVERSITY
of NORTH CAROLINA
at CHAPEL HILL

DEPARTMENTS OF MATHEMATICS AND
BIOMEDICAL ENGINEERING
INSTITUTE FOR ADVANCED MATERIALS,
NANOSCIENCE AND ENGINEERING
CAROLINA CENTER FOR INTERDISCIPLINARY
APPLIED MATHEMATICS

March 7, 2008

316A PHILLIPS HALL
CAMPUS BOX 3250
CHAPEL HILL, NC 27599-3250
<http://amath.unc.edu>

T 919.962.9606
F 919.962.9345
forest@amath.unc.edu

M. GREGORY FOREST
Grant Dahlstrom Distinguished Professor

Prof. Roland Keunings
Centre for Systems Engineering and
Applied Mechanics (CESAME)
Universite catholique de Louvain
Batiment Euler
Av. Georges Lemaitre, 4
B-1348 Louvain-la-Neuve
Belgium

Re: Submission of paper to JNNFM

Dear Roland,

We respectfully submit for consideration a manuscript titled "Stress Communication and Filtering of Viscoelastic Layers in Oscillatory Shear", by Brandon Lindley, Eddie Lee Howell, Gregory Rubinstein, Breannan Smith, me, Sorin Mitran, David B. Hill, and Richard Superfine. This topic is strongly related to your work, Gareth's, as well as Giacomini, so I do not anticipate difficulty in finding referees.

Authors 2-4 were undergraduates working with me last summer, when we discovered these phenomena. My graduate student, Brandon Lindley, did the primary work in explaining their numerical findings, and he is the corresponding author. I will stay in direct contact with Brandon as the paper is handled.

I look forward to your feedback on the work.

Sincerely,

Greg

Suggested Referees:

- Roland Keunings
- Gareth McKinley
- Randy Ewoldt
- Jeffrey Giacomini
- John Dealy

Stress Communication and Filtering of Viscoelastic Layers in Oscillatory Shear

Brandon Lindley*, Eddie Lee Howell III[†], Breannan D. Smith[‡],
Gregory J. Rubinstein[‡], M. Gregory Forest*, Sorin M. Mitran*,
David B. Hill[‡], Richard Superfine[§]

March 10, 2008

1 Abstract

We revisit a classical topic: response functions of viscoelastic layers in large amplitude oscillatory shear. Motivated by questions concerning biological layers, we focus on extreme values in boundary stress signals in a parallel plate geometry, and their dependence on material properties, layer thickness, or frequency of imposed strain. We identify a robust oscillatory structure in boundary stress signals, presented first in terms of a layer height sweep and then generalized to scaling behavior with respect to all experimental parameters. The structure consists of peaks and valleys in extreme values of shear and normal stress signals versus any parameter sweep, indicating redundant mechanisms for stress communication (by tuning to the peaks) and stress

*Applied Mathematics Program, Department of Mathematics, University of North Carolina, Chapel Hill, 27599-3250

[†]Undergraduate Researcher, Summer 2007, Department of Mathematics, University of North Carolina, Chapel Hill, 27599-3250

[‡]Cystic Fibrosis Center, University of North Carolina, Chapel Hill 27599-7248

[§]Department of Physics, University of North Carolina, Chapel Hill, 27599-3250

filtering (by tuning to the valleys). In this paper, we first restrict to a single mode nonlinear Maxwell model, where analysis renders a transparent explanation and simplified computation of the phenomena. We close with a Giesekus model simulation of coupled nonlinear partial differential equations, which is the context in which the phenomena was discovered. The analysis and simulations rely on and extend our recent studies of shear waves in a micro-parallel-plate rheometer [4, 5].

2 Introduction

The behavior of viscoelastic layers in large amplitude oscillatory shear (LAOS) has been studied in depth in the rheology literature. The methods of inquiry are varied, ranging from presumed homogeneous deformations where the problem analytically reduces to a dynamical system of ordinary differential equations [7, 12, 11], to presumed one-dimensional heterogeneous deformations where the models are coupled with systems of partial differential equations [4], to two-dimensional heterogeneity and the need for demanding numerical solver technology [6].

In LAOS, the rheological focus is typically on departures from linear responses and good metrics for capturing the onset and degrees of nonlinearity in the system. We refer to [7] and [9, 10] for a scholarly treatment of the phenomenological signature of nonlinearity in LAOS. A key diagnostic for divergence from linear behavior is Lissajous figures of shear stress (τ_{xy}) versus shear rate ($\dot{\gamma}$) [16]. In the linear regime, the $(\dot{\gamma}(t), \tau_{xy}(t))$ Lissajous figures are characterized by thin ellipses which distort in various ways in the nonlinear regime [7].

The phenomenon of interest for this paper is motivated by a biological query. There are countless examples in biology where a viscoelastic layer plays a vital mechanistic function. The work of Hosoi and co-workers has explored snail mucus and locomotion principles [8]. Our focus arises from lung biology, where mucus layers line

pulmonary pathways and serve as the medium between air from the external environment and the cilia-epithelium complex. The typical transport mechanism explored is mucociliary clearance, in which pathogens are trapped by mucus while coordinated cilia propel the mucus layer toward the larynx. However, another mechanical function explored by Tarran et al. [13] is the role of oscillatory stress in regulating biochemical release rates of epithelial cells. This discovery raises fundamental questions about the stress signals arriving at the epithelial cells from a sheared mucus layer. Air-drag stresses from either tidal breathing or cough are communicated through the mucus layer to the opposing interface, whereas cilia-induced strain generates stress at the same interface. Thus, it is natural to explore one driven interface, either by time-dependent strain or stress, and then to monitor the stress or strain communication at both interfaces.

In this paper, we impose oscillatory strain and explore interfacial stresses. This is a natural starting point for the biological application, and also happens to be the experimental configuration of finite-depth "Ferry-Stokes" viscoelastic shear waves, for which we have recently built experimental [5] and modeling [4] tools. Thus, we have ready software and analytical understanding of the coupled flow and stress waves in an oscillatory strain-driven viscoelastic layer. The studies presented here relate first to shear stress signaling, followed by the generation of normal stresses through nonlinear material properties. We focus on the upper convected nonlinearity as the common feature of all nonlinear continuum mechanical laws [14, 15]; the results remain robust in the presence of other nonlinearities, such as the Giesekus model, where these phenomena were first discovered through numerical studies. Thus we begin the discussion with a single-mode upper convected Maxwell constitutive law, for which analysis of the authors [4] can be applied; we reveal the nature of the oscillatory dependence of stress signals with respect to all parameters.

The remainder of the paper is organized as follows: We first recall the formulation

of the model, and basic mathematical properties of the solutions relevant to oscillatory strain boundary conditions from [4]. Next, we proceed to explore stress communication. Because of nonlinearity, the analogous results with imposed oscillatory stress do not follow from the strain results: a single frequency input strain yields full harmonic stress response, and vice-versa. In the "homeostatic response", where one focuses on the frequency-locked response to the periodic strain driving condition, we can work out the precise relationship between oscillatory strain-controlled and stress-controlled experiments (section 4.6). This is true only for the upper convected Maxwell model, another argument for special attention to this simplest of all nonlinear differential constitutive laws.

We organize boundary stress signals in terms of "transfer functions" which convey specific information about the response of the viscoelastic layer. The transfer functions for this paper are the extreme maximum normal and shear stress signals arriving at either plate in oscillatory strain experiments, maximized or minimized over the period of the frequency-locked response of the layer. Shear stresses oscillate with mean zero, so there is no need to track their minima. First normal stress differences of the UCM model are non-negative, so convey the bounds on normal stress generation. These transfer functions are functions of material and experimental parameters and our focus becomes the behavior with respect to each argument. One can view this strategy as an analysis of experimental parameter space. The first illustration is the behavior of the extreme boundary shear and normal stress signals for a series of experiments where the layer height is varied; we illustrate with three "model fluids" ranging from a highly elastic to a viscoelastic to a simple viscous fluid. We show that the maximum normal and shear wall stresses exhibit strong peaks at discrete depths, with a significant drop between the peaks, except in the viscous fluid limit. For the upper convected Maxwell model, the frequency-locked response is explicitly solvable for a finite depth geometry [4], and thus we have explicit formulas for all wall stress

transfer functions versus all parameters. The dependence on layer height happens to be the simplest to analyze and identify the nature of the peaks and valleys versus height. We then extend the results to all other parameters by numerical evaluation of the explicit formulas. Finally, to show robustness of the behavior, we shift to the Giesekus model. We generate parameter sweeps of the stress transfer functions, which now require numerical simulations of the governing system of nonlinear partial differential equations at each fixed parameter set, a parameter sweep of runs, followed by post-processing of the transfer functions. The oscillatory structure in these boundary stress signals is shown to persist; as mentioned earlier, this is indeed the context in which the phenomena were discovered, and the simplification to the UCM model was taken to gain an analytical understanding.

3 Mathematical Model

We recall the formulation developed in [4, 5], which is a generalization of the Ferry shear wave model [1, 2, 3] to finite depth layers and nonlinear constitutive laws. We summarize the key elements from these references in order to describe the present focus on boundary stress signals in oscillatory strain experiments. The equations of motion for an incompressible fluid are¹,

$$\rho \left(\frac{\partial \vec{v}}{\partial t} + (\vec{v} \cdot \nabla) \vec{v} \right) = \nabla \cdot \mathbf{T} \quad (1)$$

$$\nabla \cdot \vec{v} = 0, \quad (2)$$

where \mathbf{T} is the total stress tensor, \vec{v} is the fluid velocity, and ρ is the fluid density. The total stress tensor is decomposed as $\mathbf{T} = -pI + \boldsymbol{\tau}$ and then the constitutive properties of the viscoelastic material are prescribed for $\boldsymbol{\tau}$, the "extra stress tensor."

¹Throughout this paper, arrows will indicate column vectors, while bold symbols indicate tensors

We restrict attention to the simplest nonlinear constitutive law, the Upper Convective Maxwell (UCM) model, which possesses the convective nonlinearity that is common to all non-linear constitutive models. In this model, the viscoelastic properties are coarse-grained into a single elastic relaxation time (λ_0) and a single zero-shear-rate viscosity (η_0):

$$\lambda_0 \overset{\nabla}{\boldsymbol{\tau}} + \boldsymbol{\tau} = 2\eta_0 \mathbf{D}, \quad (3)$$

where \mathbf{D} is the rate-of-strain tensor, $\mathbf{D} = 1/2(\nabla\vec{v} + \nabla\vec{v}^T)$. The upper convected derivative, which makes the coupled system of flow and stress nonlinear, is defined as

$$\overset{\nabla}{\boldsymbol{\tau}} = \frac{\partial \boldsymbol{\tau}}{\partial t} + (\vec{v} \cdot \nabla)\boldsymbol{\tau} - \nabla\vec{v}^T \cdot \boldsymbol{\tau} - \boldsymbol{\tau} \cdot \nabla\vec{v}. \quad (4)$$

We assume one-dimensional shear flow in the x direction between the parallel plates and that vorticity is negligible, so that $v_y = v_z = 0$. The two parallel plates remain at heights $y = 0$ and $y = H$, with strain controls on the lower plate given by the displacement amplitude A and oscillation frequency ω . This boundary control can be stated in terms of boundary conditions on the primary velocity v_x at $y = 0$,

$$v_x(0, t) \equiv V_0 \sin(\omega t); \quad (\text{BC1}) \quad (5)$$

where $V_0 = A\omega$, while the top plate is held stationary for the purposes of this paper, which sets

$$v_x(H, t) \equiv 0. \quad (\text{BC2}) \quad (6)$$

The self-consistent reduction of stress yields $\tau_{xz} = \tau_{yz} = \tau_{zz} = 0$. The full model (2-4) reduces to the following closed system of partial differential equations for the remaining unknowns, $(v_x, p, \tau_{xx}, \tau_{xy}, \tau_{yy})$, which are functions of the gap height (y) and time:

$$\rho \frac{\partial v_x}{\partial t} = \frac{\partial \tau_{xy}}{\partial y} \quad (7)$$

$$\frac{\partial p_y}{\partial y} = \frac{\partial \tau_{yy}}{\partial y} \quad (8)$$

$$\lambda_0 \frac{\partial \tau_{xx}}{\partial t} - 2\lambda_0 \frac{\partial v_x}{\partial y} \tau_{xy} + \tau_{xx} = 0 \quad (9)$$

$$\lambda_0 \frac{\partial \tau_{xy}}{\partial t} - \lambda_0 \frac{\partial v_x}{\partial y} \tau_{yy} + \tau_{xy} = \eta_0 \frac{\partial v_x}{\partial y} \quad (10)$$

$$\lambda_0 \frac{\partial \tau_{yy}}{\partial t} + \tau_{yy} = 0. \quad (11)$$

We are only concerned with "homeostatic" responses for this study, in particular the frequency-locked response of the fluid layer to the boundary control. Thus we suppress the effects of transients and initial conditions on velocity, pressure and stress. From (11), τ_{yy} decays exponentially to zero, and from (8) any pressure gradient likewise converges rapidly to zero. In [4], a complete solution of this problem is derived resting on the observation that v_x and τ_{xy} decouple into a linear hyperbolic system once τ_{yy} is negligible, and then the remnant of nonlinearity from the upper convective derivative reduces to the solution of (8) with known functions for the velocity and shear stress. The 2x2 system (7, 9, satisfying BC1 and BC2) is solved, in the $H = \infty$ limit by Ferry et al. [1, 2, 3], and generalized to any finite H by the authors [4]:

$$v_x(y, t) = \text{Im} \left(V_0 e^{i\omega t} \frac{\sinh(\delta(H - y))}{\sinh(\delta H)} \right) \quad (12)$$

$$\tau_{xy} = \text{Im} \left(-V_0 \eta^* \delta e^{i\omega t} \frac{\cosh(\delta(H - y))}{\sinh(\delta H)} \right). \quad (13)$$

Here we have introduced the complex viscosity, $\eta^* = \eta' - i\eta''$ which, for a single-mode Maxwell fluid is,

$$\eta' = \frac{\eta_0}{1 + (\omega\lambda_0)^2} \quad (14)$$

$$\eta'' = \frac{\eta_0 \omega \lambda_0}{1 + (\omega \lambda_0)^2}. \quad (15)$$

The key complex parameter in the response functions for v_x and τ_{xy} is

$$\delta = \alpha + i\beta, \quad (16)$$

the same notation and parameter identified by Ferry in the semi-infinite layer limit, which is given for the single mode Maxwell model by:

$$\alpha = \sqrt{\frac{\rho\omega}{2\eta_0} \left(\sqrt{1 + \omega^2 \lambda_0^2} - \omega \lambda_0 \right)} \quad (17)$$

$$\beta = \sqrt{\frac{\rho\omega}{2\eta_0} \left(\sqrt{1 + \omega^2 \lambda_0^2} + \omega \lambda_0 \right)}. \quad (18)$$

This solution, though written here for the UCM model, is a special case of the solution for a general linear viscoelastic fluid [4, 1]. The real parameters α and β correspond physically to the attenuation length and wavelength described by Ferry in the semi-infinite domain problem. In the finite depth layer, our formulas resolve counter-propagating waves and thus the physical significance of α and β is not transparent in a snapshot; instead we have developed inverse characterization protocols based on microbead tracking and single particle paths [5].

We proceed now to the focus of this discussion, namely stress boundary signals. With the exact expressions for v_x and τ_{xy} , the evolution of τ_{xx} is now explicitly given by a quadrature solution of (8), where initially τ_{xx} is assumed to be zero:

$$\tau_{xx}(y, t) = 2 \int_0^t e^{(t-t')/\lambda_0} \frac{\partial v_x}{\partial y}(y, t') \tau_{xy}(y, t') dt'. \quad (19)$$

The convolution integral cannot be carried out explicitly (at least not under the weight of our pen thus far), but can be numerically evaluated. The transfer functions

of interest are then given for the UCM model by evaluation of these formulas at $y = 0$ or $y = H$. Note that since $\tau_{yy} = 0$ in the UCM model after transients have passed, the first normal stress difference $N_1 = \tau_{xx} - \tau_{yy}$ and τ_{xx} are used interchangeably until we get to the Giesekus model simulations.

4 Stress Selection Criteria

The primary focus of most studies of large amplitude oscillatory shear (LAOS) is on the dynamic (time-dependent) responses in a given experiment. The dynamic response functions sometimes presume homogeneous deformations [7] while other studies explore heterogeneity [6]. Our study admits 1-dimensional heterogeneity, but we are interested in stress information arriving at layer boundaries. For a given realization of the experiment, we extract the extreme boundary shear and normal stress signals arriving at either the driven interface or the opposing stationary interface. The wall shear stress oscillates with mean zero and the maximum and minimum values have the same magnitude, so only the maximum of shear stress is reported. The normal stress τ_{xx} is non-negative, so both extreme values are reported to convey the range of normal stress generation. These "transfer functions" are denoted: $\max_t \tau_{xy}(0, t)$, $\max_t \tau_{xy}(H, t)$, $\max_t \tau_{xx}(0, t)$, $\min_t \tau_{xx}(0, t)$, $\max_t \tau_{xx}(H, t)$, and $\min_t \tau_{xx}(H, t)$. To begin the discussion we consider $\max_t \tau_{xy}(0, t)$. Later, after we identify salient features of these transfer functions, we return to the more traditional Lissajous figures of the time-dependent stress and shear rate, and illustrate their variation with model control parameters.

4.1 Analysis of Interfacial Stress Signals

Consider the following "layer" transfer function: the maximum shear stress of the frequency-locked response, maximized over time, retaining its dependence on gap

height:

$$\max_t \tau_{xy}(y, t) = \max_t \text{Im} \left(-\delta V_0 \eta^* e^{i\omega t} \frac{\cosh(\delta(H-y))}{\sinh(\delta H)} \right). \quad (20)$$

For any fixed gap height, the maximum stress response reduces to analysis of this function as a function of the material and experimental parameters. At the lower plate, the shear stress response function is easily derived (by finding the time of maximum stress over each period $2\pi/\omega$ and then evaluating at that time):

$$\tau_{xy}^{max}(\rho, \lambda_0, \eta_0, \omega, H) = V_0 |\delta| |\eta^*| |\coth(\delta H)|. \quad (21)$$

4.2 Height-dependent oscillatory structure in shear stress signals

The simplest dependence of $\tau_{xy}^{max}(\rho, \lambda_0, \eta_0, \omega, H)$, equation (21), is with respect to H , the layer height, for which the dependence is proportional to $|\coth(\delta H)|$. Thus, the H -dependence reduces to a real-valued function of a complex argument, δH , where δ is the complex quantity defined in equations (16)-(18). For fixed material properties ρ , η_0 and λ_0 , and driving frequency ω , the dependence on H reduces to the evaluation of $|\coth(\delta H)|$ along the ray δH in the complex plane. Figure 1 provides a graph of the complex values of $\coth(\delta H)$ for a range of H in three physically distinct model fluids: a strongly elastic fluid with $\eta_0 = 1000\text{cm g/sec}$ and $\lambda_0 = 10\text{sec}$, a viscoelastic fluid with $\eta_0 = 100\text{cm g/sec}$ and $\lambda_0 = 1\text{sec}$, and a viscous fluid with $\eta_0 = 1\text{cm g/sec}$ and $\lambda_0 = 0\text{sec}$. The spiral nature of the $\coth(\delta H)$ function simply reflects the exponential behavior for real δ and the oscillatory behavior for imaginary δ . Clearly the polar angle of the complex number δ (i.e. the ray δH) determines whether the stress signals are dominated by exponential or oscillatory behavior of the \coth function. This is made precise just below.

Figure 2 plots the transfer function $\tau_{xy}^{max}(\rho, \lambda_0, \eta_0, \omega, H)$, which is proportional

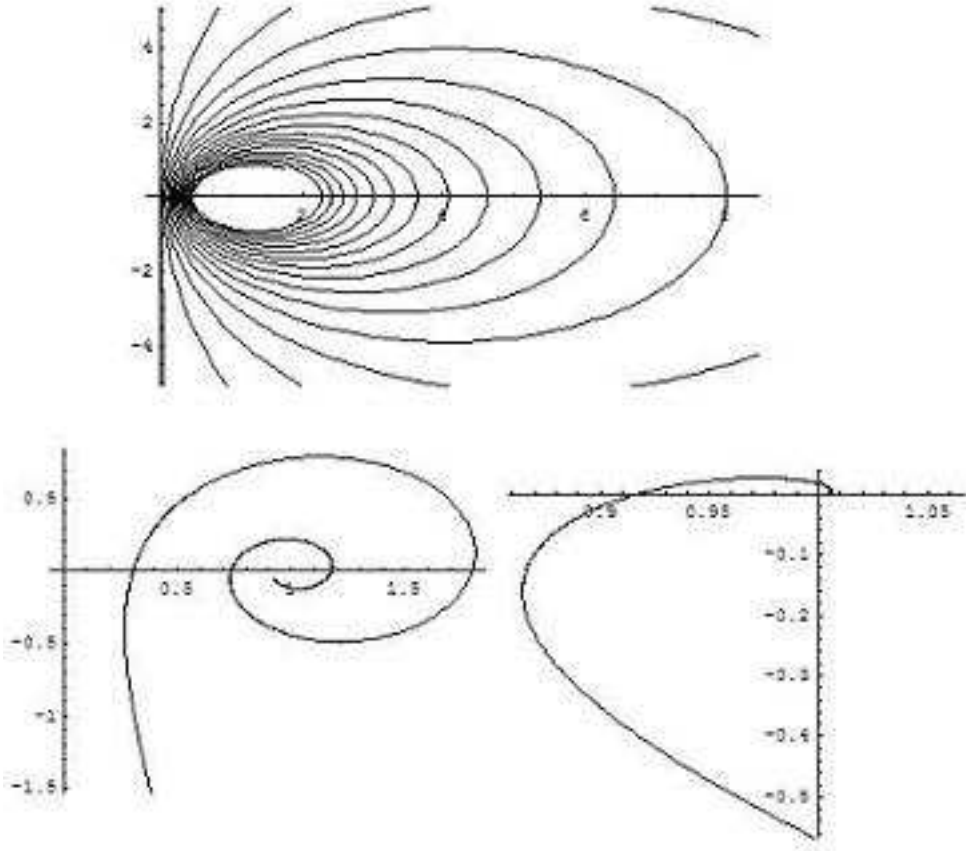


Figure 1: Evaluation of $\coth(\delta H)$ as a complex-valued function over a range $[H_{min}, H_{max}]$ for three model fluids: counter-clockwise from the top, a highly elastic fluid with Maxwell parameters $\eta_0 = 1000\text{cm g/sec}$, $\lambda_0 = 10\text{sec}$, a viscoelastic fluid with $\eta_0 = 100\text{cm g/sec}$, $\lambda_0 = 1\text{sec}$, and a fluid near the viscous limit with $\eta_0 = 1\text{cm g/sec}$, $\lambda_0 = .01\text{sec}$. Henceforth, we refer to these parameter choices as Model Fluid 1, 2 and 3. For future reference, we note that $\alpha/\beta = .0080$ for Model Fluid 1, $\alpha/\beta = .0791$ for Model Fluid 2 and $\alpha/\beta = .9391$ for Model Fluid 3.

to the modulus of the complex-valued spiral in Figure 1, for the same three model fluids. Clearly, there are oscillations versus layer height in the shear stress signal at the driven plate (in the highly elastic and viscoelastic regimes), with envelopes of the successive peaks and valleys that derive from the exact formula. The peaks and valleys of Figure 2 correspond to the apogee and perigee of Figure 1, respectively.

The apparent regularity of the locations of the peaks and valleys in the maximum plate stress signal versus H is dependent on the fluid parameters and frequency chosen in Figure 1. Note, as we approach the viscous limit, the peaks and valleys vanish. If we express $|\coth(\delta H)|$ as follows,

$$|\coth(\delta H)|^2 = \frac{\sin^2(2\beta H) + \sinh^2(2\alpha H)}{(\cos(2\beta H) - \cosh(2\alpha H))^2}, \quad (22)$$

the dual periodic and exponential dependence is transparent. If the material parameters yield α small with respect to β , for instance a model fluid with $\eta_0 \approx 100\text{cmg/s}$ with a relaxation time of approximately 1s, which renders α smaller than β by an order of magnitude, then the peaks are very regularly spaced. In a viscous fluid, such as Model Fluid 3 in Figures 1 and 2, $\alpha = \beta$ and the oscillatory structure vanishes.

From (19), we also have a closed-form expression for the first normal stress difference $N_1 = \tau_{xx}$ (since $\tau_{yy} = 0$). Fig 3 is a plot of τ_{xx}^{max} and τ_{xx}^{min} at $y = 0$, again for a range of layer depths. Note that the maxima and minima occur at the same values of H as the maximum shear stress. This property will be illustrated in more depth below.

4.2.1 Lissajous Figures

Following the work of [6, 7], Figure 4 presents Lissajous figures which show the dynamics of shear stress versus shear rate for a given model experiment. For this sweep, we present only the Lissajous figures for Model Fluid 2, but recognize that Model

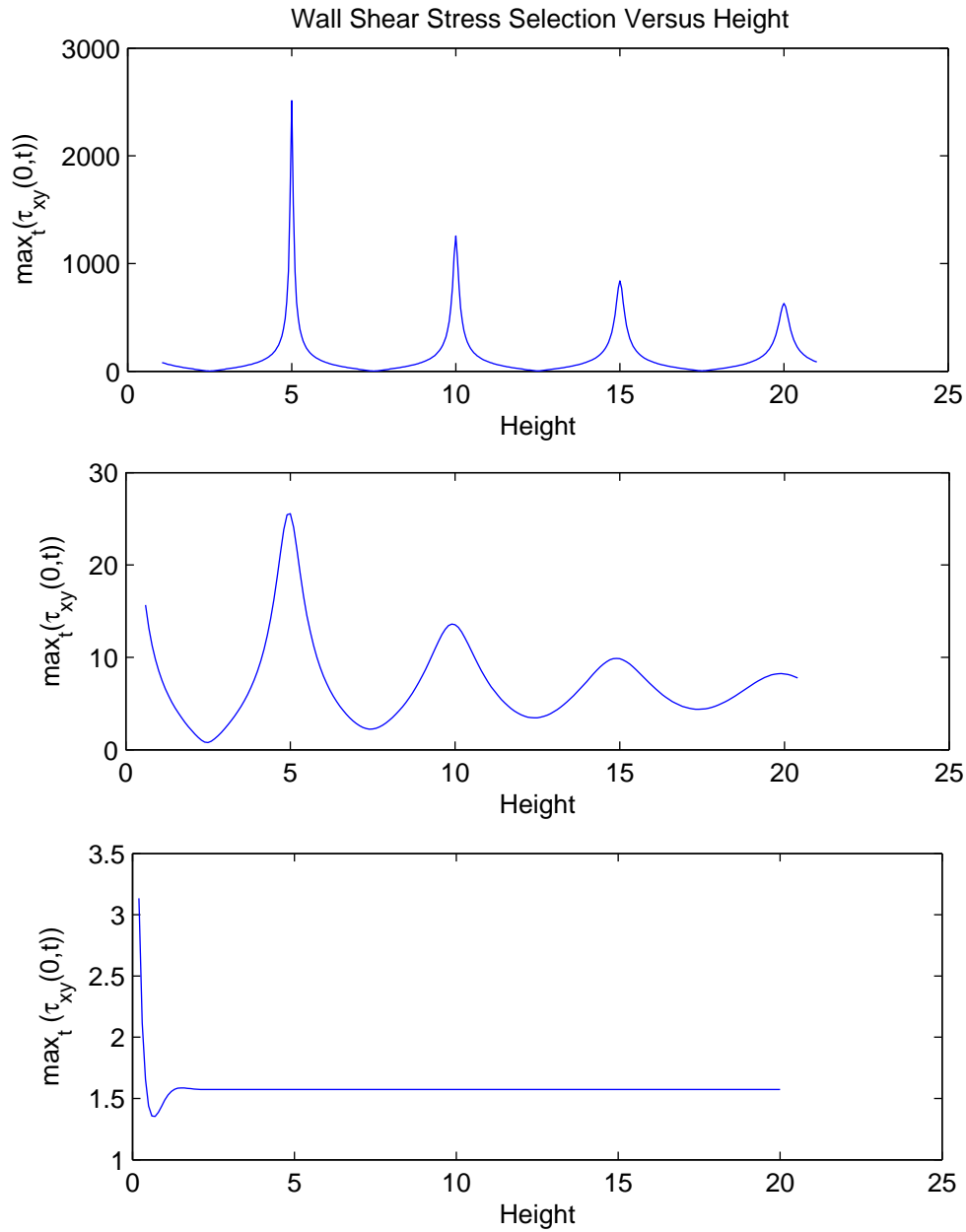


Figure 2: Maximum shear stress at the lower plate versus layer depth (equation 21) for the three model fluids. The peaks and valleys of the response function correspond to the apogee and perigee, respectively, of the spirals in Fig 1. For these runs the driving conditions are $A = .1\text{cm}$ and $\omega = 1\text{Hz}$.

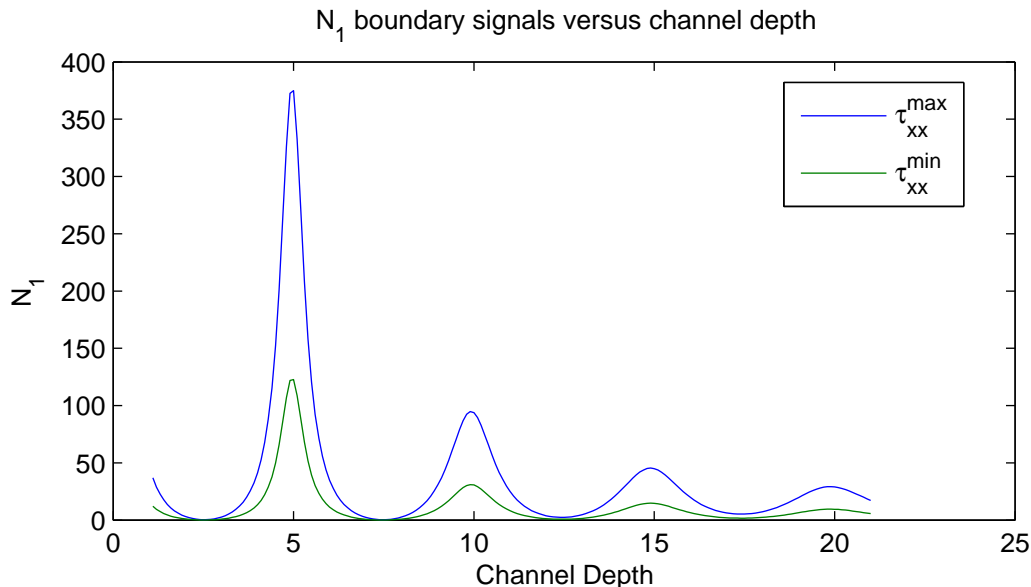


Figure 3: Maximum and minimum first normal stress difference N_1 at the lower plate versus layer depth (equation 21) for Model Fluid 2 of Figures 1 and 2 (note $\tau_{yy} = 0$ after transients have passed).

Fluid 1 will exaggerate the results of Figure 2, while Model Fluid 3 suppresses the phenomenon entirely. For linear viscoelastic fluids in a semi-infinite domain, the Lissajous figure is a slanted, thin ellipse where the slant angle is determined by the ratio β/α of the real and complex parts of δ [7], and is given as $\phi = \tan^{-1} \alpha/\beta$. In the viscous fluid limit, where $\alpha = \beta$, the slant angle of the ellipse is precisely 45 degrees. Fig. 4, also shows the extreme values of shear stress at these heights for Model Fluid 2 which are 3 of the data points in Figure 3.

Next, in Figure 5 we give the analogous Lissajous figures of the normal stress τ_{xx} versus shear rate, for the same simulations of Figure 4. The key features are: the normal stress has half the period of the shear stress and shear rate, and the extreme values are clearly non-monotone versus layer height H . Lastly, in Figure 6, we present Lissajous figures of the first normal stress difference N_1 versus the shear stress τ_{xy} . We find non-monotone behavior consistent with previous Figures, but further, oscillations in the relative extreme values of N_1 and τ_{xy} . Thus, changing the height of the layer also controls the relative magnitude of the stress components. It is also clear that the

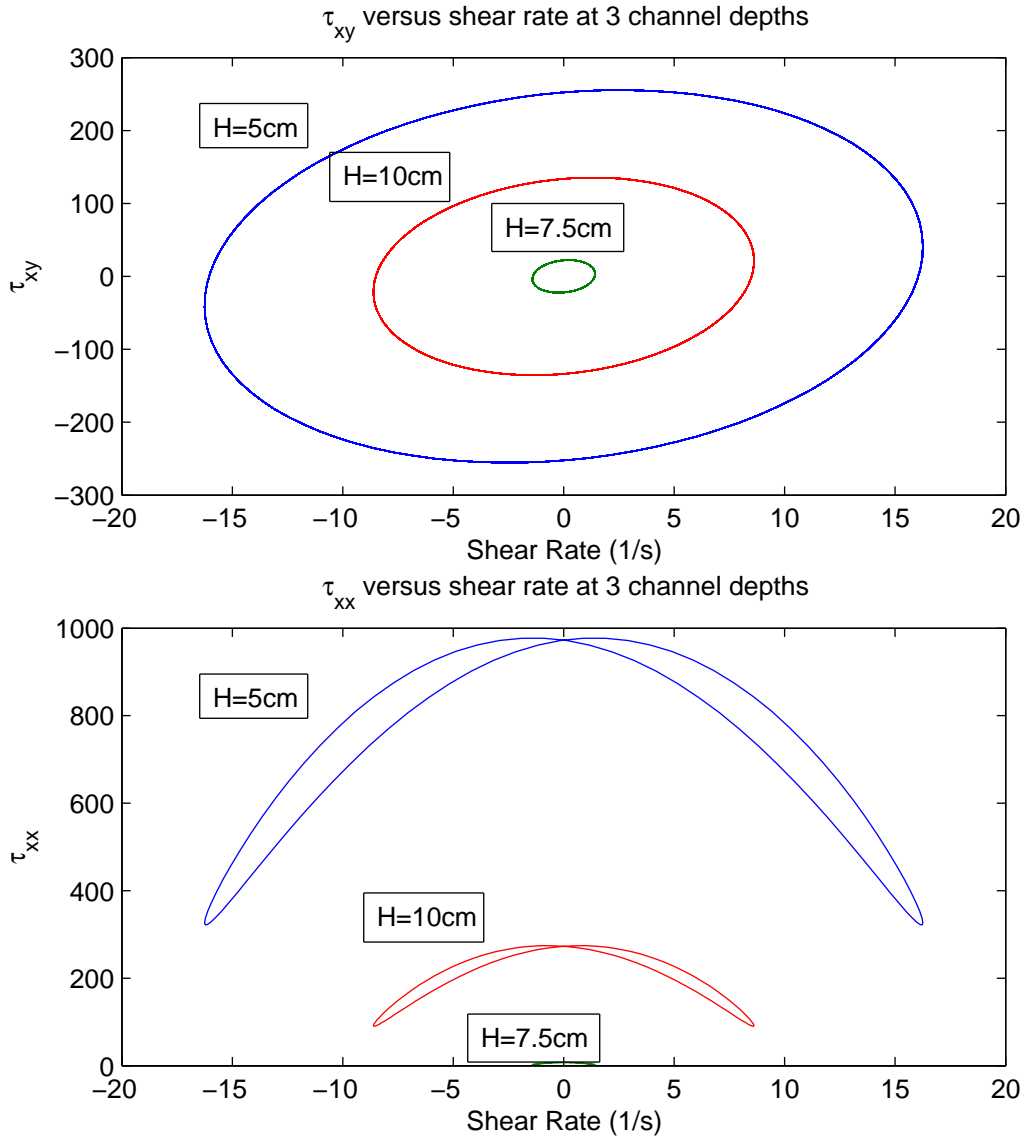


Figure 4: Lissajous figures of shear and normal stress vs. shear rate of Model Fluid 2 for three distinct layer heights, $H=5,7.5,10\text{cm}$, with a driving frequency of 1Hz and lower plate displacement of .1cm. a) Shear stress versus shear rate. b) Normal stress versus shear rate.

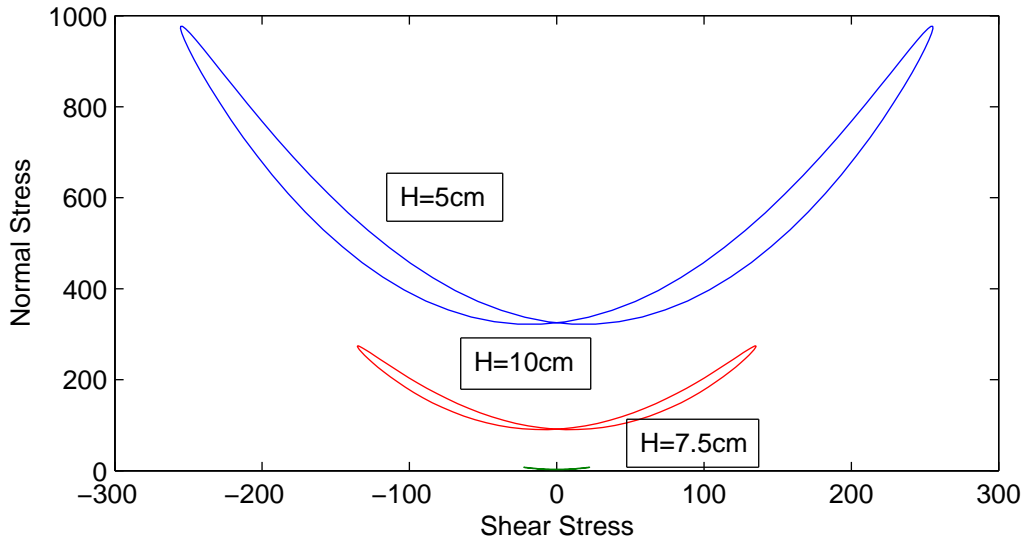


Figure 5: Time-dependent normal stress versus shear stress loops for Model Fluid 2 for the same data as Figure 4.

maxima and minima of the shear and normal stresses occur at the same times.

4.3 Frequency Sweeps

Next, we turn to the frequency-dependence of the shear and normal stress transfer functions. Their dependence on ω is more complicated than H , yet their behavior again is simply a matter of evaluating the explicit formulas (19,21). Figure 6 shows the result for Model Fluid 2 over the frequency range $0 < \omega < 2$ for $H = 10\text{cm}$. For the previous H sweep in Figure 2, we fixed $\omega = 1$, and $H = 10$ was near a peak in the shear stress transfer function. From Figure 6, it is clear that by increasing or decreasing ω from 1, the extreme interfacial stress functions for normal and shear stress walk off of the peak value, but that additional peaks occur near .5 cm and 1.5 cm. There is no need to restrict to studying the transfer of interfacial stress as a function of a single variable. Figure 7 gives the transfer function for extreme interfacial shear stress over several parameters, such as ω and H , with a range of frequency and layer height given by $\omega \in [0, 2]$ and $H \in (0, 10]$ for Model Fluid 2.

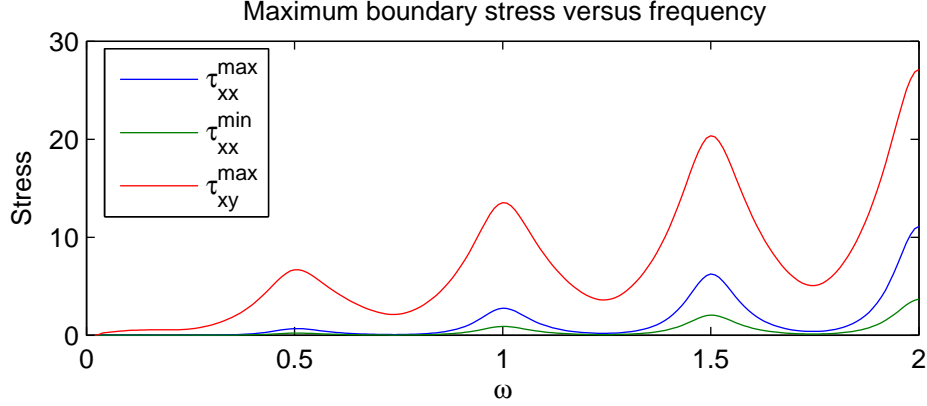


Figure 6: A frequency sweep of extreme wall shear and normal stresses for Model Fluid 2 over the frequency range $[0, 2]$.

From graphs such as Figure 7, one can find local maxima and minima of the transfer functions over ranges of the driving and fluid parameters.

4.4 Scaling behavior for wall extreme values of shear and normal stress

Before proceeding to the dependence on the UCM material parameters η_0 , λ_0 and ρ , we pause to examine the scaling behavior of the oscillatory structure versus H and ω . Namely, the *regularity* of the peaks and valleys versus H and ω is quite striking. From the analysis versus H , it is clear that the behavior is not periodic, except in the elastic limit of $\alpha \ll \beta$. The elastic solid limit is reached by letting η_0 and λ_0 become large while maintaining a constant ratio. The attenuation and wave length parameters (α and β) become:

$$\lim_{\substack{\eta_0 \rightarrow \infty \\ \lambda_0 \rightarrow \infty \\ \eta_0/\lambda_0=c}} \alpha = 0 \quad (23)$$

$$\lim_{\substack{\eta_0 \rightarrow \infty \\ \lambda_0 \rightarrow \infty \\ \eta_0/\lambda_0=c}} \beta = \omega \sqrt{\rho \lambda_0 / \eta_0}, \quad (24)$$

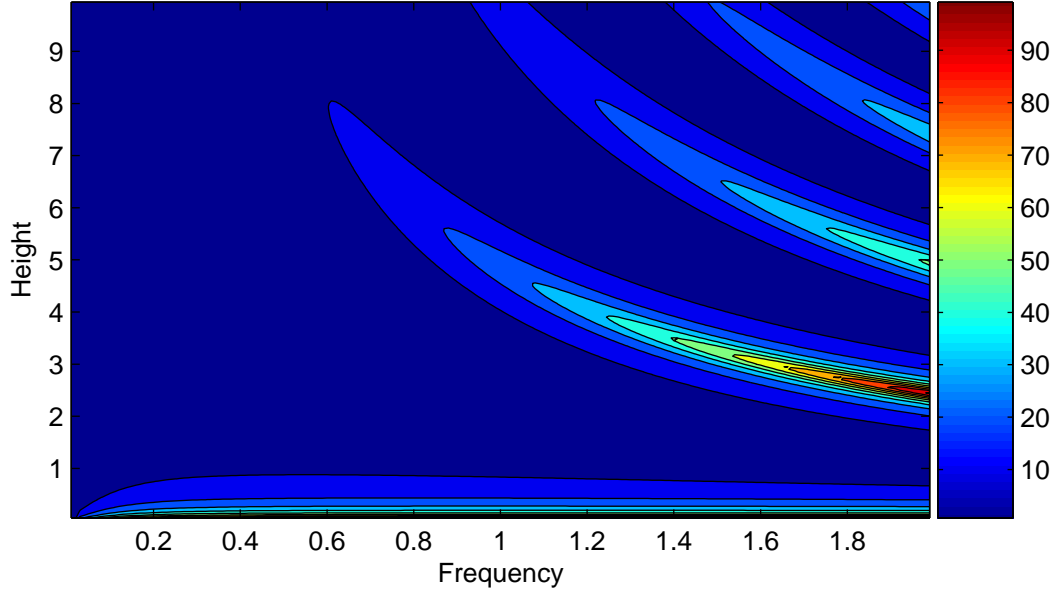


Figure 7: A parameter sweep of extreme wall shear stress for Model Fluid 2 over the range of parameters $\omega \in [0, 2]$ Hz and $H \in (0, 10]$ cm.

and the extreme shear stress transfer function, equation (21), becomes,

$$\tau_{xy}^{\max} = V_0 \beta \eta'' |\cot \beta H|. \quad (25)$$

Thus, the extreme shear stress transfer function, in the elastic limit, exhibits asymptotes at,

$$\beta = \frac{\pi}{H} k \quad k \in \{0, 1, 2, \dots\} \quad (26)$$

If we now identify the elastic wave speed,

$$c_0 = \sqrt{\frac{\eta_0}{\lambda_0 \rho}}, \quad (27)$$

then β is given by ,

$$\beta = \frac{\omega}{c_0}, \quad (28)$$

and thus the resonance condition can be restated in the elastic limit as:

$$\frac{c_0}{2\bar{\omega}H}k = 1 \quad k \in \{0, 1, 2, \dots\}, \quad (29)$$

where $\omega = 2\pi\bar{\omega}$. In terms of the frequency sweep, the fundamental frequency, denoted $\bar{\omega}_{\text{fund}}$, becomes

$$\bar{\omega}_{\text{fund}}^{\text{peak}} = c_0/2H, \quad (30)$$

which is equivalent to a period of plate oscillation that matches the round trip travel time of the elastic shear wave. Additional resonance frequencies are integer multiples of this fundamental frequency. Expressing equation (29) with respect to any of the fluid or control parameters gives a resonance condition for that value. For example,

$$H_{\text{peak}}^{\text{fund}} = c_0/2\bar{\omega}. \quad (31)$$

To extend these results from the elastic solid limit to any viscoelastic fluid, consider the non dimensional parameter α/β . Since $\alpha < \beta$, then for any viscoelastic fluid $\alpha/\beta \in (0, 1)$. As we have seen in equations (23, 24), the elastic solid limit corresponds to $\alpha/\beta = 0$, and further in the viscous limit $\lambda_0 \rightarrow 0$ it is clear that $\alpha/\beta = 1$. With respect to this parameter α/β , a measure of where a fluid is in the elastic solid to viscous limit, one could gauge the efficacy of using the elastic solid resonance condition as an estimate for the peaks and valleys of the transfer functions. Table 1 explores the usage of (31) as an estimate for the peaks and valleys of the extreme shear stress for a wide range of α/β , and confirms that as $\alpha/\beta \rightarrow 1$, the usage of (31) as a prediction of the first fundamental peak of the transfer function becomes dramatically worse.

α/β	H_{fund} Approx	H_{fund} Exact	Percent Error
.000796	.5	.49999	< .00001
.007957	.5	.4999	< .00001
.015913	.5	.4998	.0400
.026515	.5	.4995	.1001
.039726	.5	.4989	.2205
.079075	.5	.4955	.9082
.172598	5	4.819	3.756
.237477	5	4.659	7.319
.552726	5	3.820	30.89

Figure 8 gives another interpretation of the data in Table 1, by graphing the percentage error as a function of α/β in the loglog scale. The data points are fit here by a power law, which becomes a line in the loglog scale, and exhibits the nature of the walk off from pure resonance behavior as a fluid deviates from the elastic limit. In summation, for any fluid with known zero shear viscosity η_0 and relaxation time λ_0 , one can get an approximation of the fundamental layer height that will maximize stress transfer. The accuracy of this approximation can be gleaned by from Table 1. Further, by solving equation (29) for any of the variables, the following approximate scaling conditions (exact in the elastic limit) are identified:

$$\bar{\omega}_{\text{peak}}^k \approx kc_0/2H \quad (32)$$

$$H_{\text{peak}}^k \approx kc_0/(2\bar{\omega}) \quad (33)$$

$$\lambda_{\text{peak}}^k \approx k^2 \frac{1}{4H^2\bar{\omega}^2} \frac{\eta_0}{\rho} \quad (34)$$

$$\rho_{\text{peak}}^k \approx k^2 \frac{1}{4H^2\bar{\omega}^2} \frac{\eta_0}{\lambda} \quad (35)$$

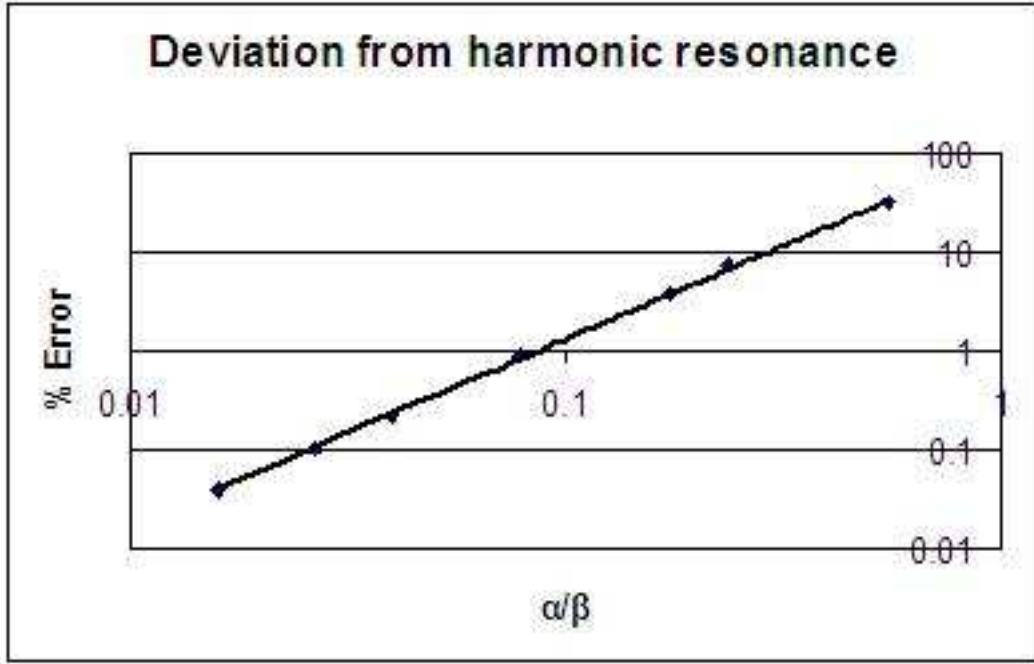


Figure 8: Percent error calculations for using equation (27) to predict peaks of the extreme shear stress for different viscoelastic fluids with given ratios α/β . The scale is loglog and thus the trend-line shown is a simple power law fit to the data.

$$\eta_{\text{peak}}^k \approx \frac{4H^2\bar{\omega}^2\lambda\rho}{k^2}. \quad (36)$$

4.5 Transfer Function Dependence on η_0 , λ_0 and ρ

We now illustrate the inferences gained in the previous section. Namely, there is an underlying oscillatory structure in the extreme values of boundary stresses with respect to all parameters in the model. Figures 9-12 show this behavior for the baseline properties of Model Fluid 2 with respect to variations in the elastic relaxation time λ_0 , the zero strain rate viscosity η_0 and the fluid density ρ . Note the stress peaks are quite well approximated by the elastic limit scaling behavior presented above, formulas (34-36).

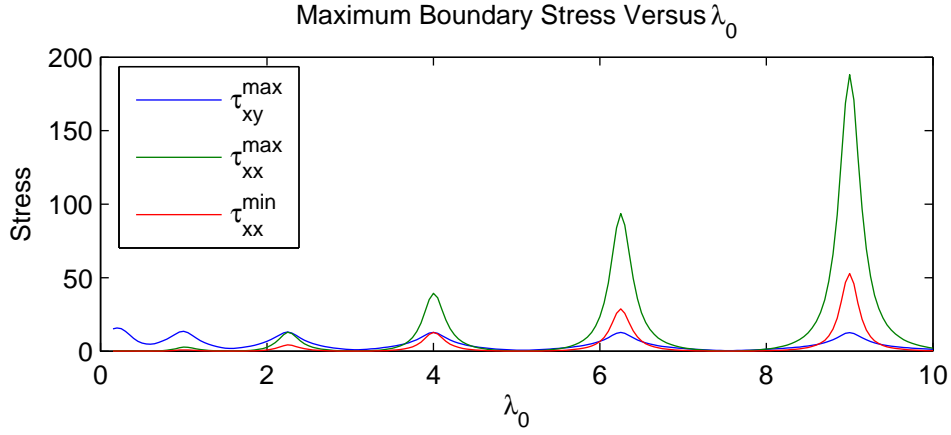


Figure 9: Relaxation time sweep of extreme boundary shear and normal stresses with respect to λ_0 variations of Model Fluid 2. We fix η_0 and ρ of Model Fluid 2 with boundary values $\omega = 1$ Hz, $A = .1$ cm and $H = 10$ cm then perform a relaxation time sweep. The elastic limit scaling prediction of the k th peak is $\lambda_{peak}^k = .25k^2$.

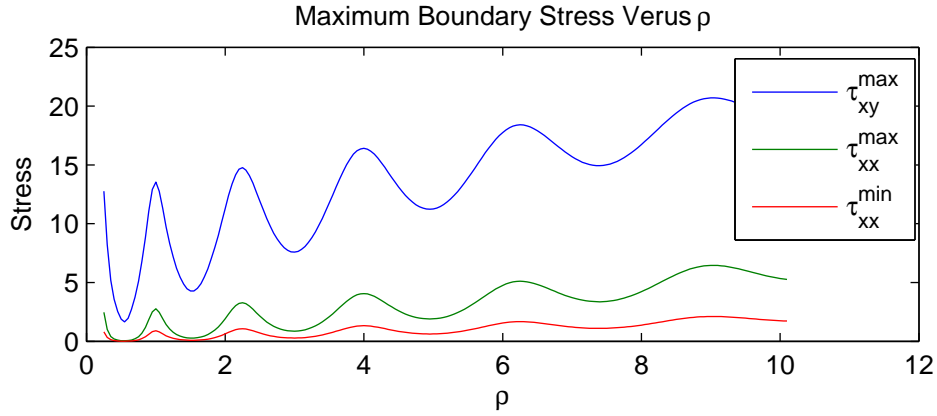


Figure 10: Density sweep of extreme boundary shear and normal stresses with respect to ρ variations of Model Fluid 2. We fix η_0 and λ_0 of Model Fluid 2 with boundary values $\omega = 1$ Hz, $A = .1$ cm and $H = 10$ cm then perform a density sweep. The elastic limit scaling prediction of the k th peak is $\rho_{peak}^k = .25k^{-2}$.

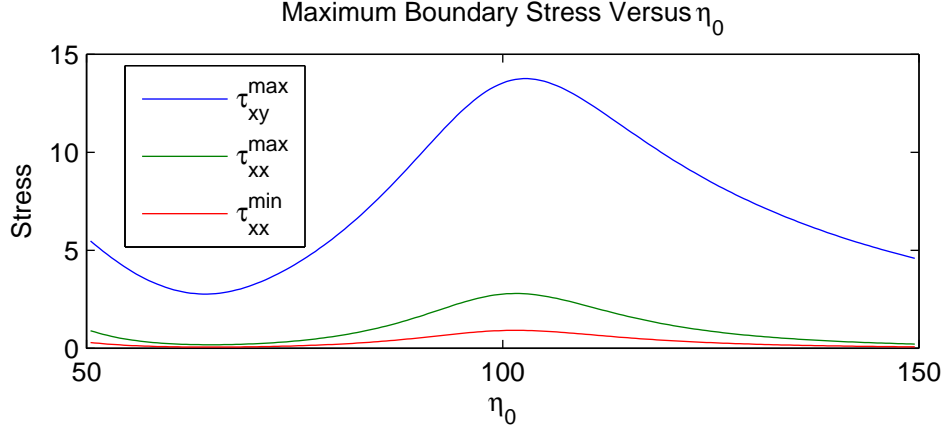


Figure 11: Zero shear-rate viscosity sweep of extreme boundary shear and normal stresses with respect to η_0 variations of Model Fluid 2. We fix ρ and λ_0 of Model Fluid 2 with boundary values $\omega = 1$ Hz, $A = .1$ cm and $H = 10$ cm then perform a zero shear-rate viscosity sweep. The elastic limit scaling prediction of the k th peak is $\eta_{peak}^k = 400k^{-2}$.

5 Transfer Function Structure for a Giesekus Fluid

Here we refer to [4] for a numerical solution to the analogous problem where the constitutive equation is given by a single mode Giesekus model. The boundary stress behavior of this paper was, in fact, discovered in this context. Figure 12 repeats the H sweep of Figure 2 for Model Fluid 2 parameters together with a mobility parameter value of .01. Figure 13 shows the result of a frequency sweep, while Figure 14 revisits the Lissajous figures of section 4.2.1 and obtains the analogous results for this model. The striking feature of Figure 14 is that nonlinearity is evident at $H = 5$ and $H = 10$, but at $H = 7.5$ the fluid exhibits the classic linear behavior (with the elliptical orbit seen in Figure 4).

The pertinent features of Figure 11 are that we see a similar height selection mechanism for the transfer of shear stress, and that the figure shows additional nonlinear structure. Note that the locations of the maxima and minima are notably different. Figure (6) contains Lissajous figures for various heights. From the Lissajous figures, it is clear that shear thinning is occurring in the Giesekus fluid at these strains.

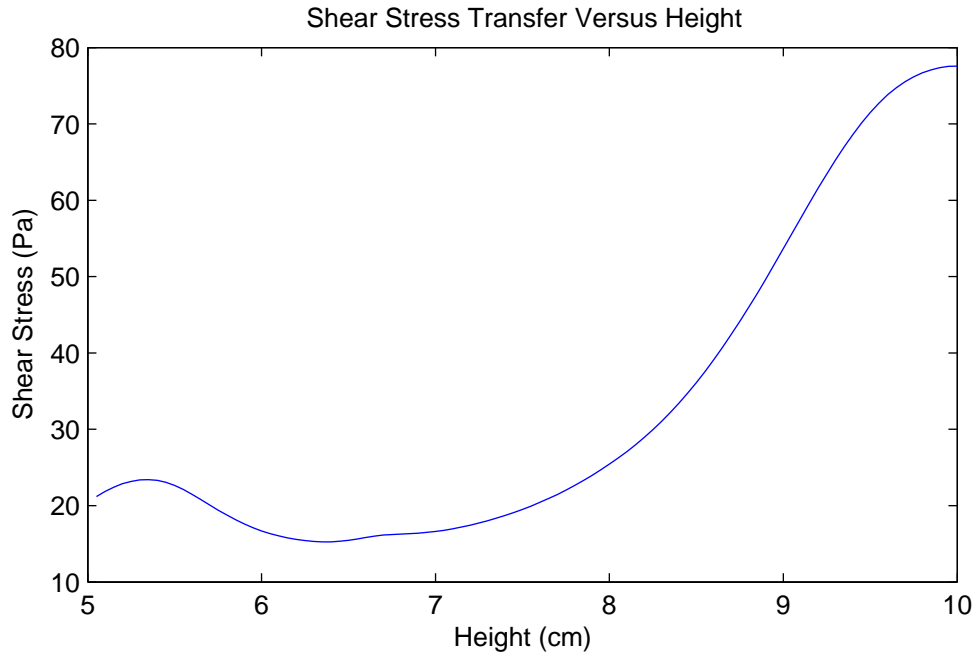


Figure 12: Maximum shear stress at the lower interface versus channel depth for Model Fluid 2 with a Giesekus mobility parameter of .01. The driving conditions here are $\omega = 1$ Hz and $A = .1$ cm.

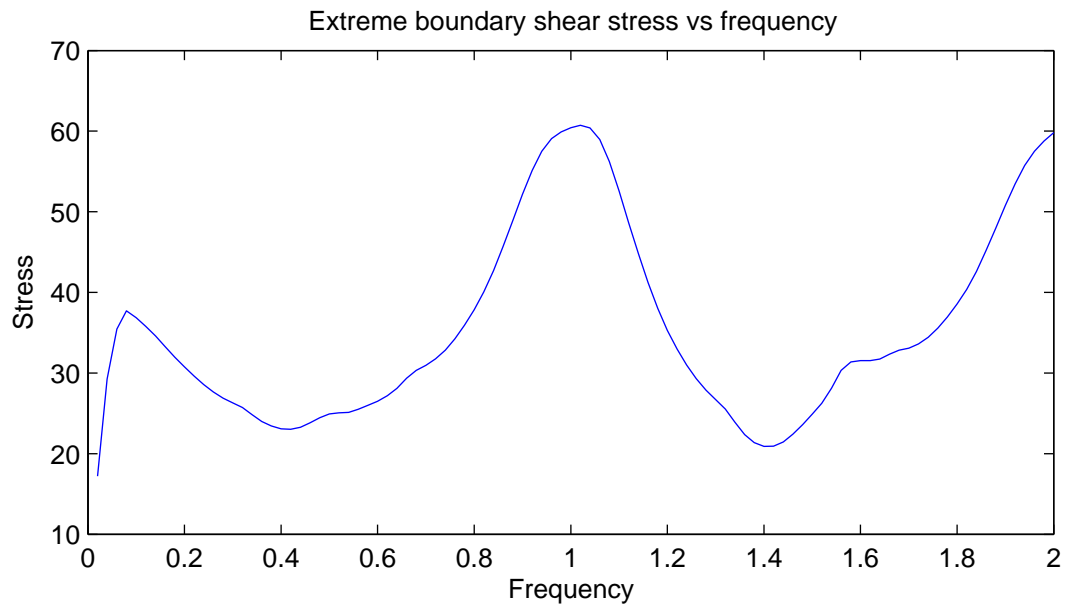


Figure 13: Maximum shear stress at the lower interface versus frequency for Model Fluid 2 with a Giesekus mobility parameter of .01. The driving conditions here are $\omega = 1$ Hz and $A = .1$ cm.

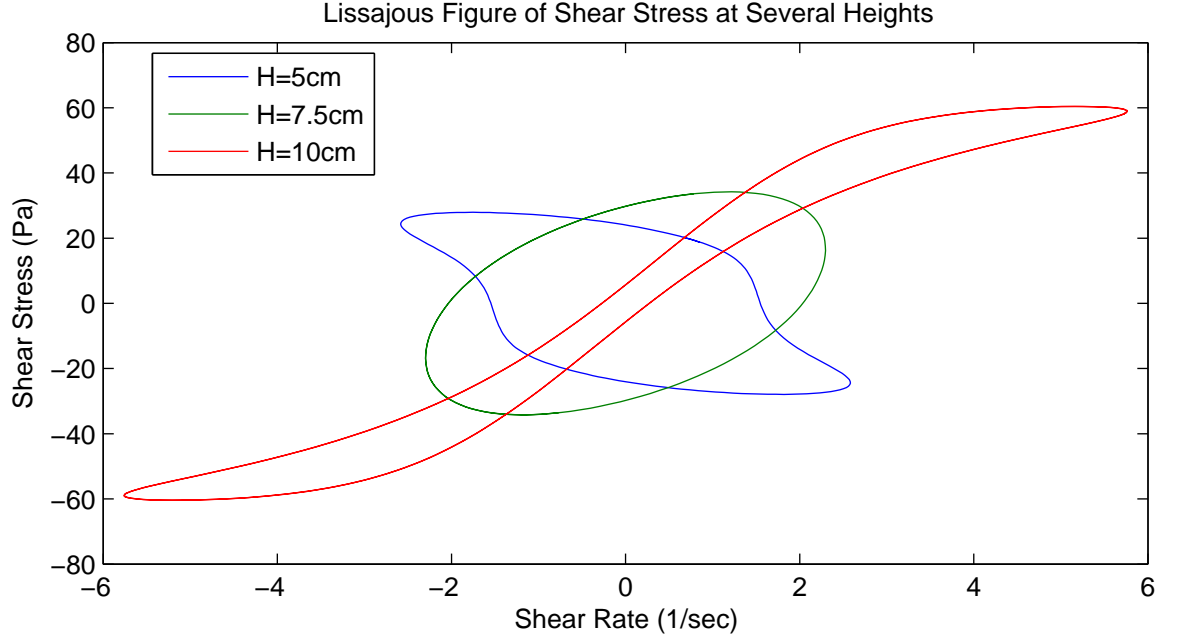


Figure 14: Shear stress versus shear rate loop for a Giesekus fluid at several heights.

6 Stress-controlled versus strain-controlled oscillatory shear

The phenomenon in question has been explored in previous sections for strain-controlled boundary conditions. Alternative boundary conditions, each modeling a different experimental protocol, consist of imposing a periodic stress or strain at either interface. For example, one can impose a periodic shear stress boundary condition at the bottom interface, retaining a stationary top boundary:

$$\tau_{xy}(0, t) = \tau_0 \sin(\omega t), \quad v_x(H, t) = 0. \quad (37)$$

It is straightforward to show that this boundary value problem is equivalent to the strain-controlled problem and solution presented above,

$$v_x(y, t) = \text{Im} \left(V_0 e^{i\omega t} \frac{\sinh \delta(H-y)}{\sinh \delta H} \right), \quad (38)$$

where V_0 is now complex valued and given by,

$$V_0 = -\frac{\tau_0}{\eta^* \delta} \tanh \delta H. \quad (39)$$

To relate the complex number V_0 above to its more natural physical interpretation as the maximum imposed velocity of the lower plate, simply take the complex modulus $|V_0|$. In this context, v_x is,

$$v_x(y, t) = \text{Im} \left(|V_0| e^{i(\omega t + \chi)} \frac{\sinh \delta(H - y)}{\sinh \delta H} \right), \quad (40)$$

where $\chi = \arg(V_0)$, demonstrating a clear equivalence of the two stress and strain controlled boundary value problems.

Perhaps more physically interesting (especially for applications to lung biology), is a stress free boundary condition at the upper interface together with an oscillatory strain at the lower interface:

$$v_x(0, t) = V_0 \sin(\omega t), \quad \tau_{xy}(H, t) = 0. \quad (41)$$

The solution is a sum of two solutions of (7-11),

$$v_x(y, t) = \text{Im} \left[e^{i\omega t} \left(V_0 \frac{\sinh \delta(H - y)}{\sinh \delta H} - V_H \frac{\sinh \delta(y)}{\sinh \delta H} \right) \right], \quad (42)$$

where the stress free condition at the upper interface determines V_H ,

$$V_H = V_0 \operatorname{sech}(\delta H). \quad (43)$$

Using a similar approach, one can determine solutions for all four sets of well-posed boundary conditions. Clearly the phenomenon persists.

7 Conclusion

The response of a viscoelastic layer in oscillatory shear has been explored with a focus on the extreme values of boundary stress signals. The phenomenon we have identified is an oscillatory structure in boundary stress signals with respect to all parameters (layer thickness, frequency of imposed shear, or material properties). This structure indicates a redundant mechanism with which to either communicate stress signals, by tuning to the peaks of the structure, or to filter stress by tuning to the valleys. Using the upper convected Maxwell model, we provide a rigorous explanation of the phenomenon, and then illustrate its persistence with a Giesekus model simulation where the results were first discovered. The relevance of these results to the biological setting of ciliary transport of mucus layers remains for future studies. The implication we have in mind is the ability of epithelial cells or cilia to mechanically sense perturbations in normal homeostatic conditions, through the variability in stress signals shown here. These perturbations may arise from mucus layer thickness variations or changes in material properties due to hydration or perhaps due to a significant deposition of pathogens at the air-mucus interface.

References

- [1] J. D. Ferry, *Studies of the Mechanical Properties of Substances of High Molecular Weight I. A Photoelastic Method for Study of Transverse Vibrations in Gels*, Rev. Sci. Inst., Vol.12, 79-82, (1941)
- [2] J. D. Ferry, *Behavior of Concentrated Polymer Solutions under Periodic Stresses*, J. Polym. Sci, 2:593-611, (1947)
- [3] J. D. Ferry, F.T. Adler, & W.M. Sawyer *Propagation of Transverse Waves in Viscoelastic Media*, J. Appl. Phys., 20, 1036-1041, (1949)

- [4] S.M. Mitran, M.G. Forest & et. al. *Extensions of the Ferry shear wave model for active linear and nonlinear microrheology*, J. Non-Newtonian Fluid Mech., to appear, (2008)
- [5] D.B. Hill, B. Lindley, M.G. Forest & S.M. Mitran *Experimental and modeling protocols from a micro-parallel plate rheometer*, UNC Preprint, 2008
- [6] R. Keunings & K. Atalik *On the occurrence of even harmonics in the shear stress response of viscoelastic fluids in large amplitude oscillatory shear*, J. Non-Newtonian Fluid Mech., 122, 107-116, (2004).
- [7] R.S. Jeyaseelan & A.J. Giacomin *Network theory for polymer solutions in large amplitude oscillatory shear*, J. Non-Newtonian Fluid Mech., Accepted, (2007).
- [8] R. H. Ewoldt, A. E. Hosoi, and G. H. McKinley, *Rheology of mucin films for Molluscan adhesive locomotion*, Abstr. Pap. Am. Chem. Soc. 231(387-PMSE), 2006
- [9] R.H. Ewoldt, A. E. Hosoi and G. H. McKinley. *Rheological Fingerprinting of Complex Fluids using Large Amplitude Oscillatory Shear (LAOS) Flows*, Nordic Rheology Conference, Stavanger, Norway, Annual Transactions of the Nordic Society of Rheology pp. 3-8 (2007)
- [10] R.H. Ewoldt, C. Clasen, A.E. Hosoi, and G.H. McKinley, *Rheological fingerprinting of gastropod pedal mucus and synthetic complex fluids for biomimicking adhesive locomotion*, Soft Matter 3(5), 634-643, 2007
- [11] Preziosi, L. , *On an invariance property of the solution to stokes first problem for viscoelastic fluids* J. Non-Newtonian Fluid Mech., 33 (2), p.225-228, Jan 1989

- [12] Preziosi, L. Joseph, D.D., *Stokes' first problem for viscoelastic fluids*, J. Non-Newtonian Fluid Mech., 25 (3), p.239-259, Jan 1987
- [13] Tarran R, Button B, Picher M, Paradiso AM, Ribeiro CM, Lazarowski ER, Zhang L, Collins PL, Pickles RJ, Fredberg JJ, Boucher RC. 2005. *Normal and cystic fibrosis airway surface liquid homeostasis. The effects of phasic shear stress and viral infections*. J. Biol. Chem. 280(42):35751-9.
- [14] R.G. Larson, **Constitutive Equations for Polymer Melts and Solutions**, Out of Print. Copies Available via personal contact rlarson@umich.edu
- [15] R. Bird, C. Curtis, R. Armstrong & O. Hassenger, **Dynamics of Polymer Fluids**, vol. 1 & 2, 2nd ed., Wiley, New York, 1987.
- [16] T.T. Tee, J.M. Dealy, *Nonlinear Viscoelasticity of Polymer Melts*, Trans. Soc. rheol. 19, 595-615, (1975)